# A DETAILED ANALYSIS OF FLOW AND HEAT TRANSFER CHARACTERISTICS UNDER A TURBULENT INTERMITTENT JET IMPINGEMENT ON A CONCAVE SURFACE

by

***Ali HAJIMOHAMMADI*** [a], ***Mehran Rajabi ZARGARABADI*** [a*], ***and Javad MOHAMMADPOUR*** [b]

[a] Faculty of Mechanical Engineering, Semnan University, Semnan, Iran
[b] School of Engineering, Macquarie University, Macquarie Park, NSW, Australia

Original scientific paper
https://doi.org/10.2298/TSCI200729334H

*A computational study is carried out of the 3-D flow field and heat transfer under a turbulent intermittent circular jet impingement on a concave surface. The control-volume procedure with the SIMPLE algorithm is employed to solve the unsteady RANS (use full form) equations. The RNG k-ε model is implemented to simulate turbulence due to its success in predicting similar flows. The numerical results are validated by comparing them with the experimental data. The effects of jet Reynolds number and oscillation frequency on the flow and heat transfer are evaluated. The profiles of instantaneous and time-averaged Nusselt numbers exhibit different trends in axial, x-directions and circumferential, s-directions. It is found that increasing frequency from 50 to 200 Hz results in considerable time-averaged Nusselt number enhancement in both axial and curvature directions. The intermittent jet at a frequency of 200 Hz enhances the total average Nusselt number by 51.4%, 40%, and 33.7% compared to the steady jet values at jet Reynolds numbers of 10000, 23000, and 40000, respectively. In addition, a correlation for the average Nusselt number is proposed depending on the Reynolds number and the Strouhal number.*

Key words: *pulsating impinging jet, heat transfer, intermittent jet, concave surface, Nusselt number, Strouhal number*

## Introduction

Impinging jets are broadly used in various industries for cooling, heating, or drying. Jet impingement provides higher heat removal for the cooling purpose in gas turbine blades or combustion chamber walls. In this method, the formation of thin hydrodynamic and thermal layers on target plates significantly increases the heat transfer performance [1-3]. Previous articles introduced various factors contributing to the higher heat transfer rate, such as the jet width, Reynolds number, jet-to-surface distance, surface curvature, and the number of jets [4, 5]. Fenot *et al.* [6] conducted a study on hot circular steady jets impingement on a concave surface. They investigated the effect of multiple jets, curvature, Reynolds number, and inlet air temperature on heat transfer. It was shown that the Nusselt number was independent of inlet jet temperatures. Mohammadpour *et al.* [7] investigated the influence of pulsating flows on jet impingement heat transfer of a concave surface. They found that a turbulent slot jet with

* Corresponding author, e-mail: rajabi@semnan.ac.ir

intermittent waves provided higher heat transfer than sinusoidal waves. Mohammadpour *et al.* [8] studied flow and heat transfer characteristics of jet impingement on a concave surface. They revealed that the jet-to-surface distance of $H/d = 0.1$ was superior to other ratios in terms of steady jet heat transfer. Mladin and Zumbrunnen [9] experimentally evaluated the effect of pulsating airflow on the local heat transfer performance from a flat surface. They found that the Nusselt number increased by 12% and 80% at the center of the target plate and the distance of five jet widths, respectively.

Pakhomov and Terekhov [10] studied the effect of different pulse forms (*i.e.*, rectangular, sinusoidal, and triangular) on the fluid-flow and heat transfer of intermittent jet impingement. They found that in the pulsed jet, for small distances between the pipe edge and the obstacle, $H/D = 6$, heat transfer around the stagnation point was enhanced when the pulsation frequency increased. However, for $H/D > 8$, an increase in frequency resulted in decreasing heat transfer. Ravanji and Zargarabadi [11] increased the averaged Nusselt number by 43-59% by adding elliptic pin fins on a concave surface under a single impinging jet. They demonstrated that pin fines had a better performance on concave surfaces with higher relative curvatures.

In recent years, oscillating jets have been employed to enhance heat transfer from impinging surfaces. A 2-D numerical study was carried out by Zargarabadi *et al.* [12] to investigate flow and heat transfer of an asymmetrical concave surface due to a sinusoidal impingement jet. It was shown that the Nusselt number of a surface with the lower curvature was higher than the other one. Twin jets were employed by Farahani *et al.* [13] to uniform the heat transfer coefficient distribution on a flat surface. They evaluated the variation of the inlet nozzle width, jet-to-surface and jet-to-jet distances, pulsation frequency, and Reynolds number on heat transfer. A relative error of 3.2% was reported between the numerical Nusselt number distribution and an optimal configuration. Alimohammadi *et al.* [14] conducted a comprehensive study on pulsating impinging jets to capture vortices and reverse vortices in the viscous sub-layer. They elucidated that pulsating flows in impingement jets were highly influenced by operating conditions, and adjusting significant parameters could remarkably enhance heat transfer. Xu *et al.* [15] verified that heat transfer was enhanced under intermittent turbulent slot impinging jets.

Liewkongsataporn *et al.* [16] demonstrated that increasing pulsating amplitudes enhanced the heat transfer rate. Li *et al.* [17] performed flow dynamics of confined sweeping jets impinging on concave surfaces at different velocities and relative curvatures. A curved shape of impingement surfaces remarkably influenced flow behavior. In addition, it was observed that the strong outer vortices promoted fluctuations of velocity even in regions far from the stagnation point. Ghadi *et al.* [18] found that pulsation flows created larger vortices compared to steady flows. The pulsation frequency played a significant role in forming, shaping, and sizing of the vortices. In terms of mixing and the transport rate, intermittent waves were superior to the pulsating flow with sinusoidal periodic patterns.

A 3-D jet impingement on a concave plate is deemed to be more similar to industrial configurations. It is noteworthy that a study on an intermittent jet impingement on a concave plate in a 3-D computational domain is a gap requiring to be explored. A key aim of the current study is the investigation of flow and heat transfer characteristics from a concave surface affected by square-wave pulsating jets. Numerical results are validated by comparing to the available experimental data. This paper captures the effects of the Reynolds number and pulsation on the Nusselt number distribution.

## Geometry and boundary conditions

Figure 1 indicates the physical domain and boundary conditions of the present study, which are similar to those in the experimental study of Fenot *et al.* [6]. The computational domain consists of a turbulent circular impinging jet at a constant distance to the concave surface, $H/d = 5.0$. The diameter of the pulsating jet is 10 mm. The impinging surface was in a semi-cylindrical shape with a diameter and length of 100 mm and 40 mm, respectively. The turbulent intensity of the circular jet is equal to 5%. The air inlet temperature is set at 298.15 K. A constant heat flux of 5000 W/m$^2$ is applied on the surface.

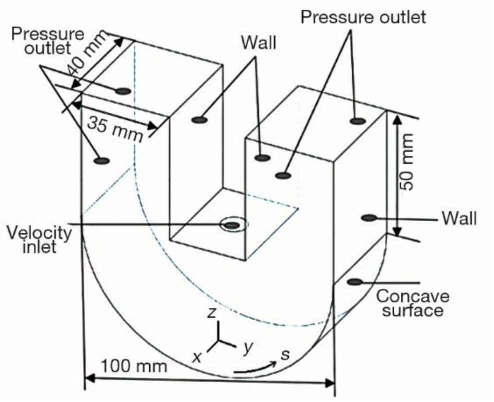


**Figure 1. Geometry and boundary condition**

The jet velocity profiles of the steady and square-shaped pulsation are shown in fig. 2. The velocity profile with square-wave pulsation is defined:

$$\frac{u_{\text{jet}}}{u_{\text{avg}}} = 2.0 \rightarrow (n) \le \frac{t}{T} < \frac{(2n+1)}{2}$$

$$\frac{u_{\text{jet}}}{u_{\text{avg}}} = 0 \rightarrow \frac{(2n+1)}{2} \le \frac{t}{T} < (n) \tag{1}$$

$$(n = 0,1,2,3,...)$$

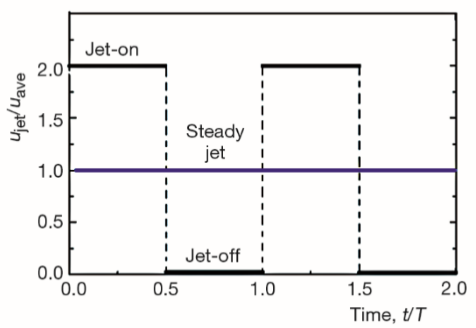


**Figure 2. Velocity profile at the jet inlet**

A completed periodic repeating pattern is called a cycle. In the square-wave pulsation, the jet inlet will be in open (first half a cycle) and closed (second half a cycle) states at various times during a cycle.

Appropriate initial conditions ($t$ = 0) for the square-wave pulsation are defined:

$$T = T_\infty, \quad k = \varepsilon = 0, \quad u = v = w = 0, \quad P = P_\infty$$

According to the air inlet temperature assumed at 298.15 K, thermophysical properties of airflow are determined as tab. 1.

**Table 1. Thermophysical properties of the flow**

| $\rho$ [kgm$^{-3}$] | $\mu$ [kgm$^{-1}$s$^{-1}$] | $k$ [Wm$^{-1}$K$^{-1}$] | $C_p$ [Jkg$^{-1}$K$^{-1}$] | Pr = $C p\mu/k$ |
|---|---|---|---|---|
| 1.184 | 1.849×10$^{-5}$ | 0.02551 | 1006.43 | 0.729 |

## Governing equations

Through employing the previous assumptions, governing equations for continuity, momentum, and energy conservations are defined by:

$$\frac{\partial \rho}{\partial t} + \frac{\partial(\rho \bar{u}_i)}{\partial x_i} = 0 \tag{2}$$

$$\frac{\partial(\rho\bar{u}_i)}{\partial t}+\frac{\partial(\rho\bar{u}_i\bar{u}_j)}{\partial x_j}=-\frac{\partial\bar{P}}{\partial x_i}+\frac{\partial}{\partial x_j}\left[\mu\left(\frac{\partial\bar{u}}{\partial x_j}+\frac{\partial\bar{u}_j}{\partial x_i}\right)-\rho\bar{u}_i'\,\bar{u}_j'\right] \tag{3}$$

$$\frac{\partial(\rho c_p\bar{T})}{\partial t}+\frac{\partial(\rho c_p\bar{u}_i\bar{T})}{\partial x_i}=\frac{\partial}{\partial x_i}\left(k\frac{\partial\bar{T}}{\partial x_i}-\rho c_p\bar{u}_i'\bar{T}'\right) \tag{4}$$

where $\bar{u}_i'\,\bar{u}'$ and $\bar{u}_i'\bar{T}'$ represent the Reynolds stress tensor and turbulence heat flux vector, respectively. The second term on the right-hand side of eq. (4) can be defined based on the simple gradient diffusion hypothesis:

$$\rho c_p\bar{u}_i'\bar{T}'=\frac{c_p\mu_t}{\sigma_t}\left(\frac{\partial T}{\partial x_i}\right) \tag{5}$$

Many turbulence models have been evaluated based on RANS [15, 17, 18] and LES [14, 19] approaches for predicting impingement heat transfer. In this paper, the turbulent flow is modeled based on the RNG *k*-*ε* model [20], and the two-layer model is implemented for walls. Due to the additional source in the dissipation equation of the RNG *k*-*ε* model, this model can predict the complexity of impinging jet flows on concave surfaces [21-23]. This turbulent model is defined by:

$$\frac{\partial}{\partial t}(\rho k)+\frac{\partial}{\partial x_j}(\rho U_j k)=\frac{\partial}{\partial x_j}\left[\left(\mu+\frac{\mu_t}{\sigma_k}\right)\frac{\partial k}{\partial x_j}\right]+P_k-\rho\varepsilon \tag{6}$$

$$\frac{\partial}{\partial t}(\rho\varepsilon)+\frac{\partial}{\partial x_j}(\rho U_j\varepsilon)=\frac{\partial}{\partial x_j}\left[\left(\mu+\frac{\mu_t}{\sigma_\varepsilon}\right)\frac{\partial\varepsilon}{\partial x_j}\right]+\frac{\varepsilon}{k}(C_{\varepsilon 1}P_k-C_{\varepsilon 2}^*\rho\varepsilon) \tag{7}$$

$$P_k=\left[\mu_t\left(\frac{\partial U_i}{\partial x_j}+\frac{\partial U_j}{\partial x_i}\right)-\frac{2}{3}\delta_{ij}\rho k\right]\frac{\partial U_i}{\partial x_j} \tag{8}$$

where $P_k$, $\mu_t$, and $\delta_{ij}$ represent the turbulence kinetic energy production, turbulent eddy viscosity, and Kronecker delta, respectively. Functions and constants of the RNG *k*-*ε* model have been expressed in [23].

## Numerical procedure

To discretize the computational domain of the present paper, a structured and non-uniform grid is considered, as shown in fig. 3. A comprehensive investigation for grid sensitivity is conducted in terms of density and size of cells through four distinctive grid measures of 299,00, 462560, 542396, and 660976 cells. According to fig. 4, a grid independency analysis is performed on the Nusselt number distribution at $H/d$ = 5 and Re = 23000. It can be observed that the grid with 542,396 computational cells provides acceptable accuracy in the prediction of local Nusselt number along the concave surface. In the aim to capture the flow and heat transfer characteristics of $Y^+ < 1$ on the concave heated surface, the density of generated cells near the wall is higher than other zones.

In the present numerical simulation, the governing conservation equations are discretized by the control volume method [24]. The SIMPLE algorithm [25] is employed for pressure-velocity coupling. The second-order upwind discretization method is adopted to consider the stability of solution convergence. The time-dependent terms are discretized using the second-order implicit scheme. The governing equations have been solved by ANSYS-FLUENT software.

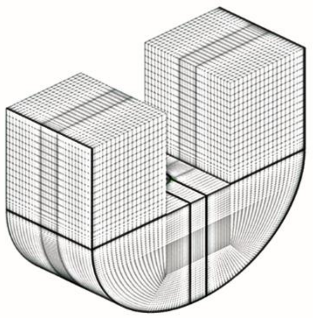

**Figure 3. Structured and non-uniform grid of the present study**

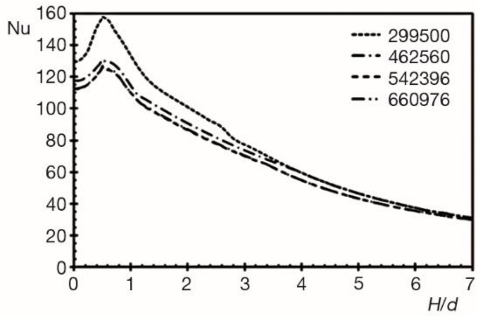


**Figure 4. Effect of grid density on the Nusselt number distribution (*H*/*d* = 5, Re = 23000)**

In the unsteady numerical simulation, the speed of convergence is dependent on the time step, and the proper time step can reduce computational time [24]. According to previous studies [24, 25], the time-step independence is checked by applying three-time steps of 1/10*f,* 1/20*f,* and 1/30*f,* implying each oscillation cycle is divided into 10, 20, and 30 time steps, respectively. The present study shows that the time step of 1/20*f* (one-twentieth of a cycle time) leads to the accurate solution with the appropriate convergence speed. Convergence in the inner iterations is achieved when the normalized residuals for continuity, momentum, and energy equations fall below $10^{-4}$, $10^{-4}$, and $10^{-6}$, respectively.

## Results and discussion

In this study, the time-averaged local Nusselt number is validated with the experimental data of Mladin and Zumbrunnen [9]. The time-averaged local Nusselt number during an oscillation period is defined:

$$\mathrm{Nu}_{\mathrm{avg}}(s) = \frac{1}{\tau}\int_0^{\tau} \mathrm{Nu}(s,t)\mathrm{d}t \tag{9}$$

Figure 5 depicts acceptable agreement between the numerical time-averaged Nusselt number distribution and experimental data [9] in both stagnation and wall jet regions.

In fig. 6, the predicted Nusselt number from a steady round jet impinging on a 3-D concave surface is compared to the experimental data [6]. This comparison reveals reasonable compatibility between the numerical prediction and the experimental data [6].

The RNG *k*-*ε* model appropriately simulates turbulent flows and heat transfer caused by impinging jets [23, 26, 27]. Hence, in the present study, the RNG *k*-*ε* model is adopted for modeling the turbulence of both steady and square-wave jets.

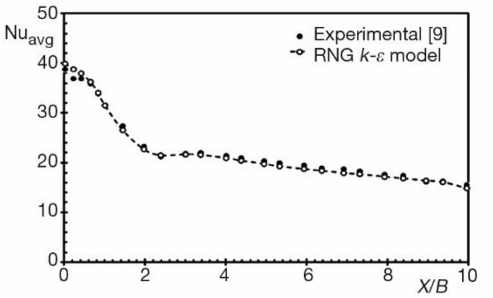


**Figure 5. Comparison of time-averaged Nusselt number with experimental results for pulsating jet [9] (Re = 5500, *f* = 41 Hz)**

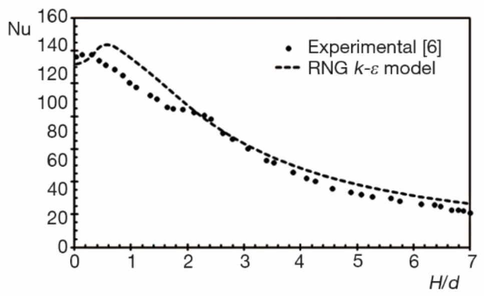


**Figure 6. comparison local Nusselt numbers with experimental results [6] for the steady jet (Re = 23000)**

In fig. 7, streamline contours of the intermittent jet (in both on/off states) are compared with the steady jet. The formation of vigorous coherent vortices near the concave surface can be observed in fig. 7(a) in the first half of the cycle (the jet is on). The coherent vortices remain and move upward in the second half of the cycle when the jet is off, fig. 7(b).

Ghadi *et al.* [18] elucidated that pulsating flows generated larger and greater coherent vorticities than steady flows in circular impinging jets. This phenomenon resulted in higher heat transfer in pulsation flows [18, 28].

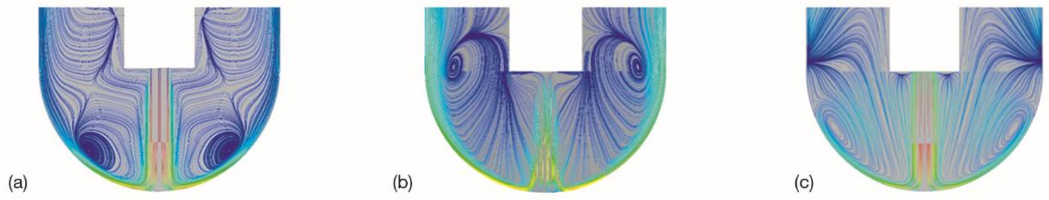


**Figure 7. Contour of streamline for the square-shaped (pulsating) jet at different time steps of a cycle (Re = 23000, *f* = 100 Hz); (a) intermittent (jet-on, *t/T* = 0.25), (b) intermittent (jet-on, *t/T* = 0.75), and (c) steady jet**

Figure 8 compares contours of velocity magnitudes between the intermittent jet (in both on/off states) and the steady jet on *x-z* and *y-z* central planes. The maximum velocity of the steady jet reaches to 37 m/s while the highest velocity of 72 m/s is obtained in the first half of the cycle for the intermittent jet. The strong vortices generated in the open state produce the maximum velocity of 23 m/s in the wall region in the closed state.

Figure 9 illustrates the distribution of instantaneous Nusselt numbers for square-wave pulsating (on/off states) and steady jets along the circumferential, *s*, and the axial, *y*, directions. According to fig. 9(a), in the first half of the cycle, Nusselt numbers along the curvature are much higher than the steady jet, especially in the impingement region. In the second half of the cycle (jet-off state), the Nusselt number of the stagnation region ($s/d < 1.2$) is significantly lower than the steady-state. However, Nusselt numbers of the off-mode in the wall jet region ($s/d > 1.2$) are higher than the steady jet.

Figure 9(b) shows that in the first half of the cycle (jet-on state), the values of the local Nusselt number along the *x*-axis for all *x/d* are higher than the Nusselt number of the

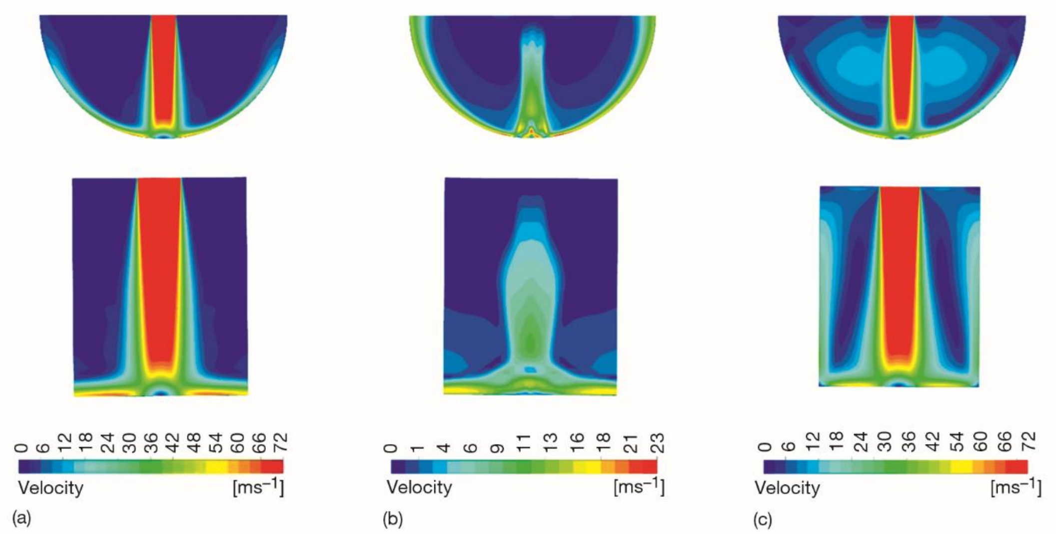


**Figure 8. Velocity magnitude of the intermittent jet (Re = 23000, *f* = 50 Hz) and steady jet, up: central *y-z* plane, down: central *x-z* plane; (a) intermittent (jet-on, *t* = *τ/4*), (b) intermittent (jet-off, *t* = *3τ/4*), and (c) steady jet**

steady jet. In the second half of the cycle (jet-off state), axial local Nusselt numbers are lower than the steady jet except in the stagnation region ($x/d \approx 0$).

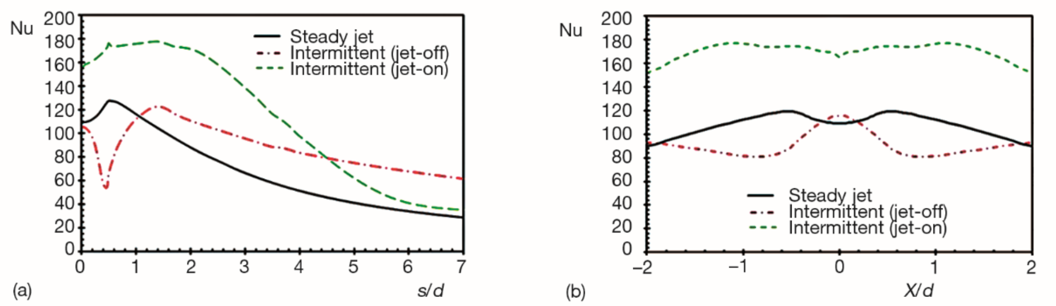


**Figure 9. Distribution of instantaneous Nusselt number (Re = 25000, *H*/*d* = 5.0, *f* = 50 Hz, jet-on *t*/*T* = 0.25, jet of *t*/*T* = 0.75); (a) circumferential and (b) axial directions**

Figure 10 exhibits the influence of oscillation frequencies on the time-averaged Nusselt number distribution. The results of the frequency variation in the range of 50-200 Hz indicate that increasing frequency enhances the time-averaged Nusselt number along the circumferential, *s*, and axial, *x*, directions in comparison with the steady jet. In addition, the local minimum Nu number in the stagnation region is disappeared.

The impact of frequency on the Nusselt number of axial directions is higher than the circumferential direction. The average Nusselt number increases by 40% for the intermittent jet compared to the steady-state. It is noted that raising the pulsation frequency to 100 and 200 Hz results in the uniform distribution of the time-averaged Nusselt number.

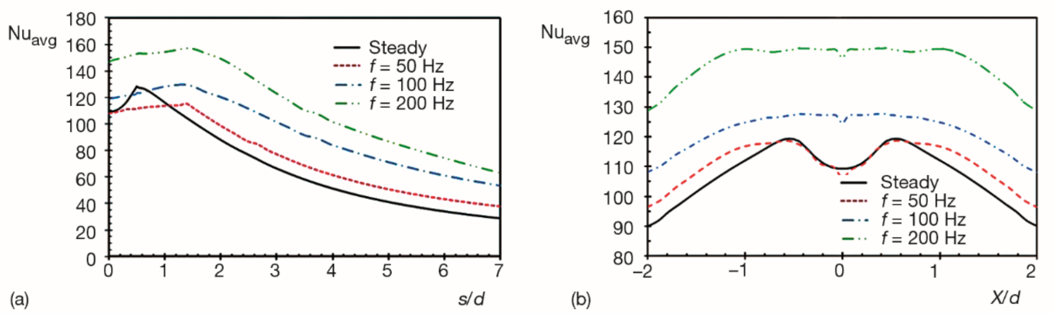


**Figure 10. Effect of frequency on the time-averaged Nusselt number (Re = 23000, *H*/*d* = 5.0); (a) circumferential and (b) axial directions**

To analyze the effects of intermittent oscillations on the formation of coherent vortices, the snapshots of velocity magnitude and streamline at different time steps of a cycle are presented in fig. 11. Comparing the snapshots at different stages shows that the formation, size, and behavior of the coherent vortices are completely different from those for the steady jet. The formation of coherent vortical structures enhances heat transfer and mixing rates [17].

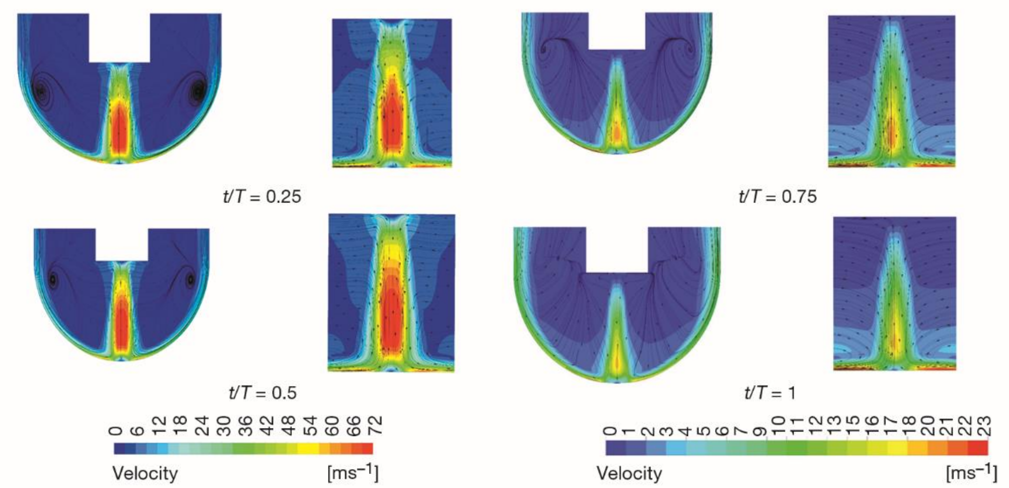


**Figure 11. Sequential snapshots of the velocity magnitude and streamline at different stages of a cycle, right: central *y*-*z* plane, left: central *x*-*z* plane (Re = 23000, *f* = 200 Hz); (a) *t*/*T* = 0.25, (b) *t*/*T* = 0.5, (c) *t*/*T* = 0.75, and (d) *t*/*T* = 0.1**

The time-and-area-averaged (total average) Nusselt number of the square-wave pulsation for the jet Reynolds number range from 10000 to 40000, and the frequency range of 50-200 Hz are tabulated in tab. 2. The area-and-time-averaged Nusselt number can be defined by:

$$\overline{\mathrm{Nu}}_{\mathrm{avg}} = \frac{1}{4\pi d}\frac{1}{\tau}\int_{-2\mathrm{d}}^{2\mathrm{d}}\int_{0}^{\tau}\mathrm{Nu}(x,\theta,t)\mathrm{d}x\mathrm{d}\theta\mathrm{d}t \tag{10}$$

**Table 2. Area-and-time-averaged Nusselt number over the concave surface and Strouhal number**

| Total average Nusselt number and Strouhal number | | | | | | |
|---|---|---|---|---|---|---|
| Frequency of jet [Hz] | Re = 10000 | | Re = 23000 | | Re = 40000 | |
| | St | Nu | St | Nu | St | Nu |
| Steady | – | 31.86 | – | 58.69 | – | 89.65 |
| 50 | 0.032 | 40.11 | 0.014 | 68.76 | 0.008 | 100.15 |
| 100 | 0.064 | 42.68 | 0.028 | 73.18 | 0.016 | 107.34 |
| 200 | 0.128 | 48.24 | 0.056 | 82.18 | 0.032 | 119.87 |

According to tab. 2, the increment of the total average Nusselt number is due to increasing the frequency of the square-wave jet at three Reynolds numbers. It is observed that the intermittent jet with 200 Hz frequency enhances the total averaged Nusselt number by 51.4%, 40%, and 33.7% than the steady jet at the Reynolds number of 1000, 23000, and 40000, respectively. The Strouhal number is a dimensionless number representing oscillating flow mechanisms. It can be seen that increasing the Strouhal number results in higher Nusselt number values. The maximum enhancement of 19.72 is obtained in the total average Nusselt number when the Strouhal number increases from 0.008 to 0.032 at the Reynolds number of 40000.

In addition, the total average Nusselt number over a concave surface was dependent on the jet Reynolds number, jet-to-surface distance ratio, and the relative impingement surface curvature [29]. However, in this study, this parameter can be expressed:

$$\overline{\mathrm{Nu}}_{\mathrm{avg}} = C\mathrm{Re}^{m}\ \mathrm{St}^{n} \tag{11}$$

From the regression analysis, the constant and exponents are defined:

$$\overline{\mathrm{Nu}}_{\mathrm{avg}} = 0.04\ \mathrm{Re}^{0.7976}\ \mathrm{St}^{0.1317} \tag{12}$$

Accordingly, the average Nusselt number is directly affected by the Reynolds and Strouhal numbers. It can be postulated that the Strouhal number, $fd/u_{\mathrm{avg}}$, has a slight impact than the Reynolds number on the averaged Nusselt number. Equation (12) accurately calculates the average Nusselt number for the Reynolds numbers range between 10000 and 40000 and frequency range from 50 to 100 Hz with the maximum deviation of 2%.

Figure 12 presents the effect of Reynolds number on the temperature distribution over the concave surface at the jet-on and jet-off states. It is observed that the concave surface temperature is reduced by increasing the Reynolds number for both jet-on and jet-off states. As the Reynolds number is raised, a reduction in the surface temperature becomes apparent. By referring to fig. 12, it can be seen that the temperature downstream of the concave surface is high, and the injected flow in the first half of the cycle can only reach the stagnation region.

## Conclusions

This paper was concentrated on the 3-D numerical simulation of a square-wave pulsation impinging jet. A computational investigation was performed to study the turbulent flow and heat transfer from a cylindrical concave surface. The effects of jet Reynolds number (10,000 < Re < 23,000) and the pulsation frequency (50 Hz < $f$ < 200 Hz) on instantaneous and time-averaged Nusselt numbers were investigated.

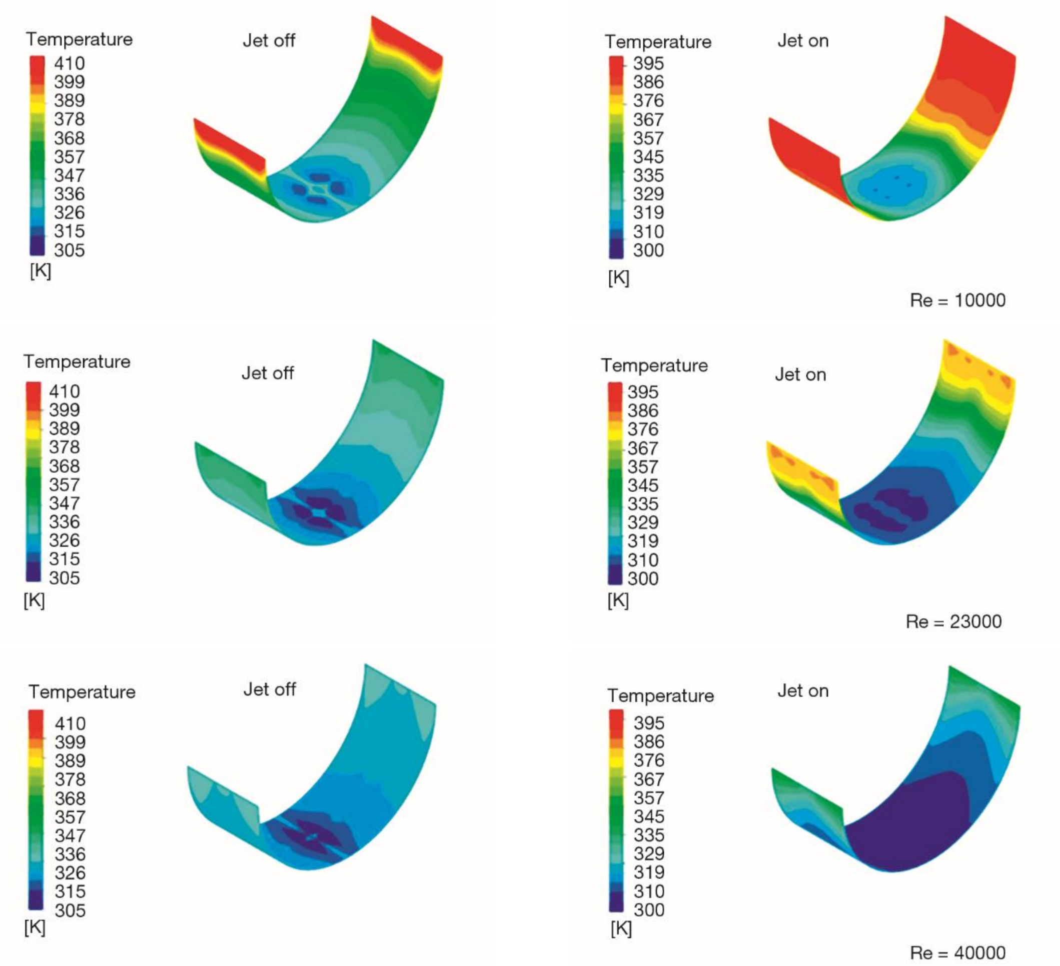


**Figure 12. Effect of Reynolds number on the temperature distribution on the concave surface (*f* = 50 Hz jet-on *t/T* = 0.25, jet of *t/T* = 0.75)**

Compatibility between the numerical findings and the experimental data verified that the RNG $k$-$\varepsilon$ model was appropriate in predicting the turbulent flow and heat transfer caused by pulsating and steady jets.

In the first half of the cycle, the formation of strong coherent vortices was observed in the vicinity of the wall. The generated vortex was adequately strong to produce a maximum velocity of 23 m/s in the wall jet region in the second half of the period.

The profiles of instantaneous and time-averaged Nusselt numbers showed different behavior in axial, $x$- and circumferential, $s$-directions. The impact of oscillation frequency on the Nusselt number along the axis was higher than that in the circumferential, $s$-direction.

The local Nusselt number at the stagnation point was enhanced by increasing the pulsating frequency. Increasing the frequency to 100 and 200 Hz caused uniform distributions of the time-averaged Nusselt number, and the local minimum Nusselt number disappeared at the stagnation point.

The intermittent jet at a frequency of 200 Hz enhanced the total average Nusselt number by 51.4%, 40%, and 33.7% than the steady jet at the Reynolds numbers of 10000, 23000, and 40000, respectively.

A correlation equation was proposed for the total average Nusselt number based on the Reynolds and Strouhal numbers. It was observed that $\overline{\mathrm{Nu}}_{\mathrm{avg}}$ was dependent on $\mathrm{Re}^{0.7976}$ and $\mathrm{St}^{0.1317}$.

## Nomenclature

$C_p$ – specific heat in constant pressure [$\mathrm{Jkg^{-1}K^{-1}}$]
$D$ – impingement surface diameter [m]
$d$ – jet diameter [m]
$f$ – the frequency of pulsating [Hz]
$H$ – jet to target distance [m]
Nu – Nusselt number (= $HD/k$)
$\mathrm{Nu}_{\mathrm{avg}}$ – local time-averaged Nusselt number
$\overline{\mathrm{Nu}}_{\mathrm{avg}}$ – total average Nusselt number
$P$ – static pressure [Pa]
$P_\infty$ – ambient static pressure [pa]
$P_k$ – turbulence kinetic energy production
Pr – Prandtl number (= $C p\mu/k$)
Re – Reynolds number (= $\rho u_{\mathrm{jet}}D/\mu$)
St – Strouhal number (= $fd/u_{\mathrm{ave}}$)
$s$ – circumferential direction [m]
$k$ – thermal conductivity [$\mathrm{Wm^{-1}K^{-1}}$]
$T$ – temperature [K]
$T_\infty$ – ambient temperature [K]
$t$ – time [s]
$U, u, v, w$ – velocity [$\mathrm{ms^{-1}}$]
$u_{\mathrm{jet}}$ – jet velocity [$\mathrm{ms^{-1}}$]
$u_{\mathrm{avg}}$ – time-average velocity [$\mathrm{ms^{-1}}$]
$\overline{u_i' u_j'}$ – Reynolds stress
$x_i$ – spatial co-ordinates [m]
$Y^+$ – dimensionless wall distance
$x, y, z$ – Cartesian co-ordinates
$c, m, n$ – corelation constants

*Greek symbols*

$\tau$ – period [s]
$\rho$ – density [$\mathrm{kgm^{-1}}$]
$\varepsilon$ – dissipation rate of turbulent kinetic energy [$\mathrm{m^2s^{-3}}$]
$\mu$ – laminar viscosity [$\mathrm{kgm^{-1}s^{-1}}$]
$\mu_t$ – turbulent viscosity [$\mathrm{kgm^{-1}s^{-1}}$]
$\sigma_\varepsilon, \sigma_k$ – turbulent Prandtl number for $k$-$\varepsilon$ density [$\mathrm{kgm^{-3}}$]
$\delta_{ij}$ – Kronecker delta
$C_{\varepsilon1}, C^*_{\varepsilon2}$ – $k$-$\varepsilon$ equation constants

*Subscripts*

$j$ – jet

## References

[1] Pakhomov M. A., Terekhov V. I., Numerical Study of Fluid Flow and Heat Transfer Characteristics in an Intermittent Turbulent Impinging Round Jet, *Int. J. Thermal Sci., 87* (2015), Jan., pp. 85-93
[2] Jiang, Z., *et al.*, Numerical Simulation of Flow and Heat Transfer from Slot Jets Impinging on a Cylindrical Convex Surface, *Journal of Thermal Science, 20* (2011), 5, pp. 460-466
[3] Qiu, D., *et al.,* On Heat Transfer and Flow Characteristics of Jets Impinging onto a Concave Surface with Varying Jet Arrangements, *Journal of Thermal Analysis and Calorimetry*, *141* (2020), 1, pp. 57-68
[4] Fenot, M., *et al.*, Local Heat Transfer Due to Several Configurations Of Circular Air Jets Impinging on a Flat Plate with and without Semi-Confinement, *International journal of thermal sciences*, *44* (2005), 7, pp. 665-675
[5] Ahmadi. H., *et al.*, Numerical Modeling of a Turbulent Semi-Confined Slot Jet Impinging on a Concave Surface, *Thermal Science*, *19* (2015), 1, pp.129-140
[6] Fenot, M., *et al*, An Experimental Study on Hot Round Jets Impinging a Concave Surface, *International Journal of Heat and Fluid Flow, 29* (2008), 4, pp. 945-956
[7] Mohammadpour, J., *et al.*, Effect of intermittent and sinusoidal pulsed flows on impingement heat transfer from a concave surface, *International Journal of Thermal Sciences*, *76* (2014), Feb., pp. 118-127
[8] Mohammadpour, J., *et al.*, Heat Transfer Under Composite Arrangement of Pulsed and Steady Turbulent Submerged Multiple Jets Impinging on a Flat Surface, *International Journal of Thermal Sciences*, *86* (2014), Dec., pp. 139-147
[9] Mladin, E. C., Zumbrunnen, D. A., Local Convective Heat Transfer to Submerged Pulsating Jets, *International Journal of Heat and Mass Transfer*, *40* (1997), 14, pp. 3305-3321
[10] Pakhomov M. A., Terekhov V. I., RANS Simulation of the Effect of Pulses form on Fluid Flow and Convective Heat Transfer in an Intermittent Round Jet Impingement, *Energies, 13* (2020), 15, 4025

[11] Ravanji, A., Zargarabadi, M. R., Effects of Elliptical Pin-Fins on Heat Transfer Characteristics of a Single Impinging Jet on a Concave Surface, *International Journal of Heat and Mass Transfer*, *152* (2020), May, 119532
[12] Zargarabadi, M. R., *et al.*, Numerical Analysis of Turbulent Flow and Heat Transfer of jet Sinusoidal Pulsed impinging on an asymmetrical concave surface, *Applied Thermal Engineering, 128* (2018), Mar., pp. 578-585
[13] Farahani, S. D., *et al.*, Optimization Arrangement of Two Pulsating Impingement Slot Jets for Achieving Heat Transfer Coefficient Uniformity, *Journal of Heat Transfer*, *138* (2016), 10, 102001
[14] Alimohammadi, S., *et al.*, On the Numerical-Experimental Analysis and Scaling of Convective Heat Transfer to Pulsating Impinging Jets, *International Journal of Thermal Sciences*, *98* (2015), Dec., pp. 296-311
[15] Xu, P., *et al.*, Turbulent Impinging Jet Heat Transfer Enhancement Due to Intermittent Pulsation, *International Journal of Thermal Sciences*, *49* (2010), 7, pp. 1247-1252
[16] Liewkongsataporn, W., *et al.*, Pulsating Jet Impingement Heat Transfer Enhancement, *Drying Technology*, *26* (2008), 4, pp. 433-442
[17] Li, Z., *et al.*, Experimental Investigation of Flow Dynamics of Sweeping Jets Impinging Upon Confined Concave Surfaces, *International Journal of Heat and Mass Transfer, 142* (2019), Oct., 118457
[18] Ghadi, S., *et al.*, Experimental Study of Formation and Development of Coherent Vortical Structures in Pulsed Turbulent Impinging Jet, *Experimental Thermal and Fluid Science*, *74* (2016), June, pp. 382-389
[19] Yu, M., *et al.*, Large Eddy Simulation of Coherent Structure of Impinging Jet, *Journal of Thermal Science*, *14* (2005), 2, pp. 150-155
[20] Kharoua, N., LES stUdy of the Combined Effects of Groups of Vortices Generated by a Pulsating Turbulent Plane Jet Impinging on A Semi-Cylinder, *Applied Thermal Engineering*, *114* (2017), Mar., pp. 948-960
[21] Yakhot, V., *et al.*, Development of Turbulence Models for Shear Flows by a Double Expansion Technique, *Physics of Fluids A: Fluid Dynamics*, *4* (1992), 7, pp. 1510-1520
[22] Ahmadi, H., *et al.*, Numerical Investigation of Semi-Confined Turbulent Slot Jet Impingement on a Concave Surface Using an $Al_2O_3$-Water Nanofluid, *Applied Mathematical Modelling*, *40* (2016), 2, pp. 1110-1125
[23] Speziale, C. G., Thangam, S., Analysis of an RNG Based Turbulence Model for Separated Flows, *30* (1992), 10, pp. 1379-1388
[24] Sharif, M. A. R., Mothe, K. K., Parametric Study of Turbulent Slot-Jet Impingement Heat Transfer from Concave Cylindrical Surfaces, *International Journal of Thermal Scienc*es, *49* (2010), 2, pp. 428-442
[25] Patankar, S. V., *Numerical Heat Transfer and Fluid Flow*, CRC Press, Boca Raton, Fla., USA, 1980
[26] Demircan, T., Turkoglu, H., The Numerical Analysis of Oscillating Rectangular Impinging Jets, *Numerical Heat Transfer, Part A: Applications*, *58* (2010), 2, pp. 146-161
[27] Behera, R. C., *et al.*, Numerical Study of Interrupted Impinging Jets for Cooling of Electronics, *IEEE Transactions on Components and Packaging Technologies*, *30* (2007), 2, pp. 275-284
[28] Xu, P., *et al.*, Heat Transfer and Entropy Generation in Air Jet Impingement on a Model Rough Surface, *International Communications in Heat and Mass Transfer*, *72* (2016), Mar., pp. 48-56
[29] Afroz, F., Sharif, M. A. R., Numerical Study of Turbulent Annular Impinging Jet Flow and Heat Transfer from a Flat Surface, *Applied Thermal Engineering*, *138* (2018), June, pp. 154-172

Paper submitted: July 29, 2020
Paper revised: April 25, 2021
Paper accepted: May 5, 2021